THE RELATIONSHIP BETWEEN CRYSTALLOGRAPHIC ORIENTATION AND THE PASSIVITY AND BREAKDOWN OF BERYLLIUM

M.A. Hill, J.F. Bingert*, R.S. Lillard
Materials Corrosion and Environmental Effects Laboratory
Materials Science and Technology Division, MS G755
Los Alamos National Laboratory
Los Alamos, NM 87545

*Mechanical Fabrication Section, MST-6

ABSTRACT

The voltage which corresponded to the onset of pitting corrosion for S200D beryllium (Be) was found to decrease logarithmically with increasing chloride concentration according to the relationship: $E_{pit} = -0.067\log[Cl^-] - 1.01$. The corrosion pits formed in Be were not hemispherical but rather the same size and shape of individual grains. In addition, parallel plates of unattacked Be could be found inside the pits indicating that pit initiation or propagation was influenced by the orientation of the grain. Preliminary orientation imaging microscopy (OIM) data, which provided color contrast maps of the microtexture of polycrystalline S200D, indicated no relationship between the susceptibility of a grain to initiation and the orientation of the grain although no corrosion pits were found to initiate in the family of planes associated with the [100] direction. Potentiodynamic polarization curves for Be single crystal showed some relationship between corrosion rate and passive current density with crystal orientation.

INTRODUCTION

For many materials, the susceptibility of single crystals to pitting corrosion has been shown to be related to crystallographic orientation. In the case of fcc Al(1) and bcc Fe(2) single crystals the close-packed planes ((111) and (110) respectively) have been found to be the most susceptible to pitting corrosion while in hcp Zn(3) the close-packed plane (0001) has been found to be the most resistant to pitting corrosion. Although surface preparation(4) and growth direction(5) may play a role in these results, one might conclude that a polycrystalline material may be engineered with a preferred texture to minimize the effects of pitting corrosion. Until recently, the only method for investigating the relationship between micro-texture (the orientation of specific grains in a polycrystalline material) and pitting corrosion has been manually generated and indexed back scattered electron diffraction (BSED) patterns (Kikuchi patterns) or electron channel patterns(4). Unfortunately these patterns are often weak and the method is labor intensive. Therefore, practically, these methods are not capable of generating a statistically significant population.

With the development of orientation imaging microscopy (OIM)(6, 7) it is now possible to rapidly establish the specific orientation of numerous individual grains in a polycrystalline material thus allowing statistically significant orientation populations in engineering materials to be examined. OIM maps are generated with a computer software program from back-scattered electron Kikuchi patterns (BSEKP) collected in the scanning electron microscope (SEM)(8, 9). The method by which the data are collected is system specific. In our system, operating the SEM in spot mode, a BSEKP for a single point on the sample is displayed on a phosphor screen that is placed inside the vacuum chamber in front of the sample. The sample is inclined 30^o with respect to the incident beam to collect sufficient back-scattered electrons. The BSEKP is captured with a silicon intensifier camera that is focused on the phosphor screen via a leaded window in the vacuum

chamber. The heart of the system is a pattern transform software program that analyzes the digitized image based on look-up tables of allowable interplanar spacings for the crystal. By stepping the electron beam over the sample surface (with a field emitting gun spatial resolutions as low as 200 nm are obtained) orientation with respect to position is obtained. The most widely used data output is the OIM color-contrast map. This map displays local orientation on the sample surface as gradients of color. The specific orientation of any one point (or color) on the sample surface is easily determined from a reference stereographic triangle which relates color to crystallographic orientation.

In this investigation OIM was used in conjunction with other techniques to examine the relationships between crystallographic orientation and the passivity and breakdown of beryllium (Be).

EXPERIMENTAL METHODS

The samples used in this study were fabricated from either Brush-Wellman S200D grade Be discs or zone refined single crystals. S200D grade Be is a powder product which is the most commonly used form of beryllium. Table 1 displays the composition of three grades of Be. The main difference between these grades of Be are the concentrations of BeO, iron, and aluminum (Al). Powder products are manufactured by comminuting vacuum cast ingots followed by grinding or milling to produce powder. In this process, a thin oxide layer forms around the Be powder particles resulting in a high BeO content. The grain size of the S200D material was on the order of 10 - 20 μm which is characteristic of powder products as the BeO particles pin grain boundaries and retard grain growth. The grain size of ingot material is typically on the order of 100 - 200 μm .

Table I Typical chemistries for Brush-Wellman S200D powder-prep Be (S200D), cast (ingot) Be, and zone refined single crystal Be (zone). Be concentration is quoted as the minimum allowable, all other species are quoted as the maximum.

	Be (at%)	BeO (at%)	Al (ppm)	C (ppm)	Fe (ppm)	Mg (ppm)	Si (ppm)	other (ppm)
S200D	98.0	2.0	3000	2800	3400	1500	1500	750
ingot	99.3	0.05	725	700	1400	-	400	200
zone	99.99	< 0.01	18	-	< 4	-	< 130	270

Electrical leads were connected to the back of samples with silver paint and epoxy. These leads were encapsulated in glass before mounting the samples in epoxy. Be samples for OIM studies were ground with successively finer grits of SiC paper followed by polishing on a wheel with diamond paste. The final polish was done using 0.3 μm diamond paste followed by a chemi-mechanical polish in colloidal silica (pH 10). Microhardness indents were then placed in the OIM sample to fix an area of interest. This area of interest was then mapped optically (under polarized light) and then with OIM. Typical OIM maps were generated at a step size of 2 μm for an area measuring approximately 200 μm by 100 μm. After characterizing the surface in this manner, the sample was immersed in a 1 M NaCl solution (ambient aeration) for a sufficient time to allow the initiation of as many discrete pits as possible while avoiding gross propagation.

Beryllium samples used in potentiodynamic polarization experiments were ground to 400 grit using SiC paper. Potentiodynamic polarization curves were generated in deaerated solution at a scan rate of 0.1 mV/s after monitoring the open circuit potential for one hour to ensure steady state. The solutions used in this investigation were prepared

from deionized water and consisted of: NaCl, pH 2 H_2SO_4, 0.5 M boric acid / 0.05 M sodium borate buffer (pH 7.2), and pH 12.5 sodium hydroxide.

Single crystal experiments were conducted the surfaces of: (0001) the basal plane, {1*1*00} the prismatic family of planes, and {11*2*0} the family of planes 90^o to prismatic (where an *italicized* indicie is negative). Orientation was confirmed with the Laue backreflection method.

RESULTS AND DISCUSSION

It has been shown that Be is passive between pH 2 and 12.5 and susceptible to pitting corrosion in chloride solution(10). Figure 1 shows potentiodynamic polarization curves for S200D beryllium in deaerated NaCl solutions ranging in concentration from 10^{-4} to 1 M Cl^-. For Cl^- concentrations below 1 M, anodic polarization of the sample was characterized by a region of passivity followed by a logarithmic increase in the current density which corresponded to the onset of pitting corrosion. In deaerated 1 M Cl^-, pitting at the OCP was observed The voltage which corresponded to the onset of pitting corrosion, E_{pit}, was found to decrease logarithmically with increasing chloride concentration according to the relationship:

$$E_{pit} = -0.067\log[Cl^-] - 1.01 \qquad [1]$$

where E_{pit} is in volts vs. SCE and $[Cl^-]$ is the concentration of chloride in Molarity (Figure 2). A similar relationship between E_{pit} and chloride concentration has been noted for aluminum(11) and stainless steel(12). . A typical scanning electron micrograph of the corrosion pits found in S200D beryllium following a polarization experiment in 0.01 M NaCl solution is presented in Figure 3. This micrograph is also representative of the corrosion pits found after pitting at the OCP. The corrosion pits in Be have the same size and shape as the Be grain morphology. Moreover, the pits are not hemispherical and parallel plates of unattacked Be could be found inside the pits. Similar attack has been observed in hcp zinc single crystals(3).

A typical OIM contrast map and the corresponding stereographic triangle for Be S200D are presented in Figure 4a. Ordinarily, each family of planes in the stereographic triangle would be represented by a discrete color (red, green, or blue). As the OIM map is a color contrast map, a one-to-one correlation between a specific grain and the stereographic triangle can be made. Unfortunately , we were not capable of showing color in this in this publication. The microhardness indents used to fix a specific area of interest, several distinguishing grains, and oxide inclusions are pointed out in this map for reference. The ability of OIM to analyze large populations of grains is evident from the contrast map in Figure 4a is evident as the orientations of approximately 800 individual grains are shown. The polarized light micrograph for a portion of this sample after immersion in 1 M NaCl for 100 s is presented in Figure 4b. Polarized light allows the grain structure to be easily identified without the need for etching as seen in this figure. However, small differences between orientation can not be discerned and, as a result, some grain boundaries are not visible in this micrograph.

The relationship between pit initiation and grain orientation was determined by first immersing the sample in 1 M NaCl solution (ambient aeration) at the open circuit for a short period of time (on the order of seconds to several minutes). This procedure was followed by examination under polarized light (Fig 4b) to detect pit initiation. This cycle was repeated until approximately 10-20% of the grains were associated with a corrosion pit. As seen in Figure 4b, this procedure avoided gross propagation of pitting corrosion (i.e. pit diameters were on the order of 5-10 μm). After 40 minutes of immersion, approximately 100 -150 corrosion pits were found on the sample. Of these pits, only 27 were found to initiate entirely with the grain boundaries of individual grains and away from the hardness indents. The remainder of the corrosion pits sites were fairly uniformly distributed

between oxide inclusions and grain boundaries. The orientations of the 27 grains that were associated with discrete initiation sites were tabulated and the results are represented in Figure 5. Each P in the stereographic triangle shown in Figure 5 designates an orientation that was associated with a discrete corrosion pit. As seen in this stereographic triangle the initiation sites were fairly randomly distributed across the stereographic triangle with the exception of the [100] direction. No corrosion pits were found to initiate in this family of planes. Although the statistical significance of this must be verified, it is worth noting that that bulk texture analysis revealed no preferred orientation.

To compliment the OIM analysis of pit initiation in polycrystalline material, the passivity and breakdown of Be single crystals is currently under investigation. Potentiodynamic polarization curves for (0001), {1*1*00}, and {11*2*0} surfaces as a function of solution pH are presented in Figures 6 through 8. Although the pitting potential in pH 2 H_2SO_4 solution (due to SO_4^{-2}) for the single crystal material is identical to S200D, both the {1*1*00}, and {11*2*0} surfaces exhibited lower open circuit potentials, and higher corrosion current densities than observed in the S200D and (0001) material. Moreover, while the S200D and (0001) material were spontaneously passive in pH 2 H_2SO_4 solution, an active to passive transition was observed in both the {1*1*00}, and {11*2*0} single crystal surfaces. While the corrosion current densities for all material types were similar in pH 7.2 borate buffer solution, a reproducible anodic peak in the (0001) material was observed. In addition, in both the pH 7.2 buffer solution and the pH 12.5 NaOH solutions the passive current density for the {11*2*0} surface was consistently higher than those measured for the other materials. Currently we are generating potentiodynamic polarization curves for the single crystal material as a function of Cl^- concentration to determine whether or not the pitting potential for Be is a function of crystallographic orientation.

CONCLUSIONS

The size and morphology of the corrosion pits in polycrystalline Be indicated that pit initiation or propagation was influenced by the orientation of individual grains.

Orientation imaging microscopy maps of polycrystalline S200D Be and post immersion optical microscopy found no correlation between pit initiation sites and crystallographic orientation of specific grains. Therefore, altering the bulk texture of polycrystalline Be will not the materials corrosion resistance to pitting corrosion.

Although pit initiation in polycrystalline Be may not be influenced by local orientation, pit propagation may be.

Potentiodynamic polarization curves for (0001), {1*1*00}, and {11*2*0} single crystal material found some differences in open circuit potential, passive current densities, corrosion current densities and active to passive transitions as a function of crystallographic orientation.

ACKNOWLEDGMENTS

Work on this project was performed under the auspices of the University of California for the United States Department of Energy contract W7405-ENG36. The authors acknowledge the continued support of Doug Kautz and the Surveillance Project Office. The authors would also like to thank George Carlson, Brett Kniss, Gary Devine (LLNL), Jim Oldani (LLNL), and Bill Moddemann (Pantex) for helpful discussions.

REFERENCES

1. M. Yasuda, F. Weinberg, D. Tromans, *Journal of the Electrochemical Society*, **137**, 3708 (1990).
2. J. Kruger, *Journal of the Electrochemical Society*, **106**, 736 (1959).
3. R. Guo, F. Weinberg, D. Tromans, *Corrosion*, **51**, 356 (1995).
4. G. Palumbo, A. M. Brennenstuhl, F. S. Gonzalez, in *Application of Accelerated Corrosion Tests to Service Life Prediction of Materials, ASTM STP 1194* , G. Cragnolino, N. Sridhar, Eds., p. 252, ASTM, Philadelphia (1994).
5. R. M. Latinision, H. Opperhauser, *Corrosion*, **27**, 509 (1971).
6. S. I. Wright, *Journal of Computer Assisted Microscopy*, **5**, 819 (1993).
7. S. I. Wright, B. L. Adams, *Metallurgy Transactions A*, **23A**, 759 (1992).
8. J. A. Venables, C. J. Harland, *Philosophical Magazine*, **35**, 1317 (1973).
9. D. J. Dingley, K. Z. Bab-Kishi, *Microscopy and Analysis*, **17**, May-July (1997).
10. M. A. Hill, D. P. Butt, R. S. Lillard, *Journal of the Electrochemical Society*, **145**, 2799 (1998).
11. Z. Szklarska-Smialowska, *Pitting Corrosion of Metals*, 221, NACE, Houston, TX (1986).
12. H. P. Leckie, H. H. Uhlig, *Journal of the Electrochemical Society*, **113**, 1262 (1966).

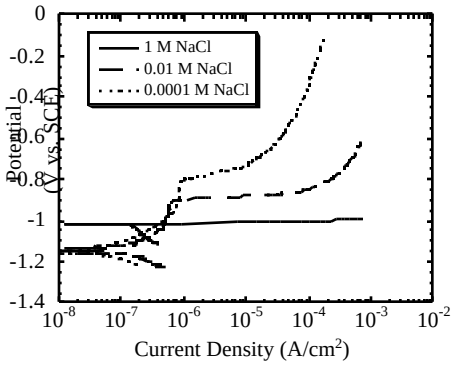

Figure 1 Potentiodynamic polarization curves for S200D Be as a function of chloride concentration showing a decrease in pitting potential with an increase in chloride concentration.

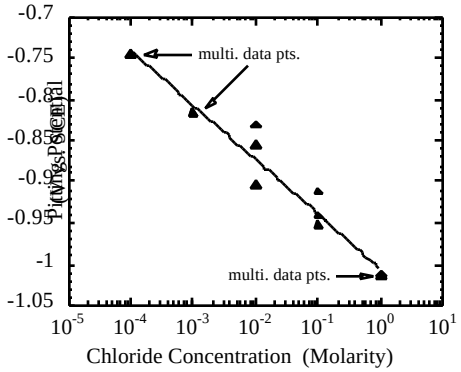

Figure 2 Pitting potential as a function of chloride concentration displaying a logarithmic relationship between E_{pit} and $[Cl^-]$.

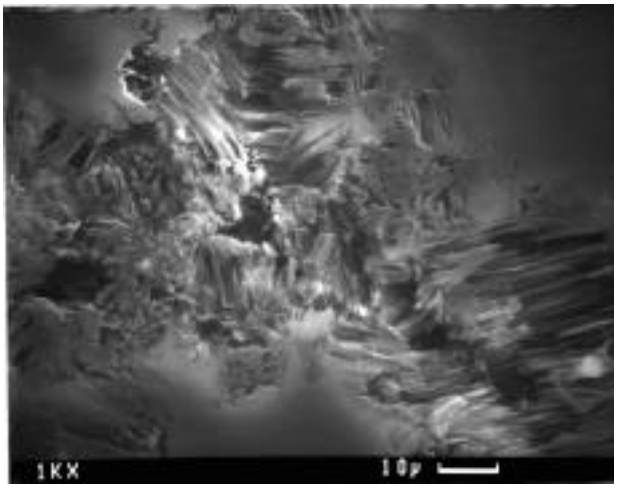

Figure 3 SEM micrograph of a corrosion pit in S200D Be showing parallel plates of Be left behind after pit propagation ceased. The size of any one set of parallel plates is consistent with the grain size in this material (about 10-40 angstroms).

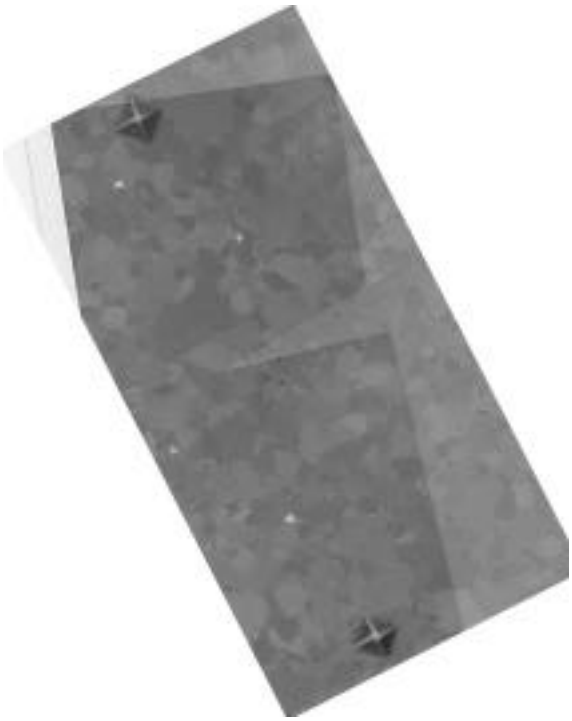

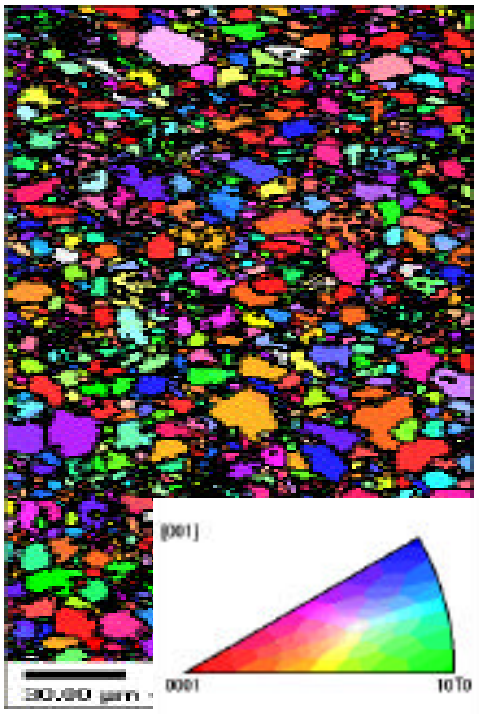

Figure 4a Polarized light micrograph of S200D grade Be prior to immersion with feducial marks and **, 4b** orientation imaging microscopy map of the same area in 4a and stereographic triangle. Grain size of this material is 10 to 30 μm.

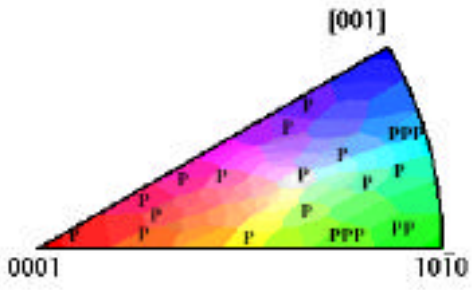

Figure 5 Stereographic triangle for Be S200D sample shown in Figures 4a and 4b. Each **P** designates an orientation that was associated with a discrete corrosion pit.

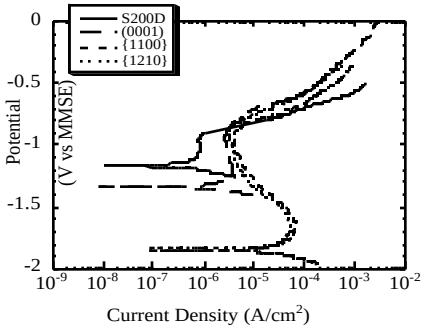

Figure 6 Potentiodynamic polarization curves for S200D Be and (0001), {1*1*00}, and {11*2*0} single crystal Be samples in pH 2 H_2SO_4.

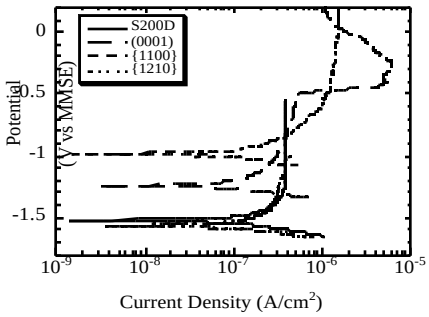

Figure 7 Potentiodynamic polarization curves for S200D Be and (0001), {1*1*00}, and {11*2*0} single crystal Be samples in pH 7.2 borate buffer.

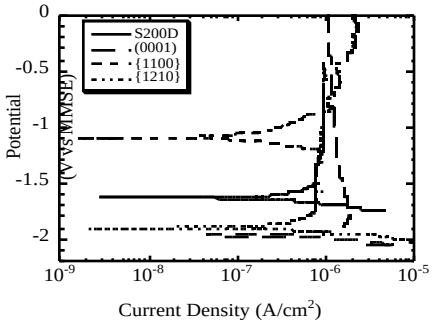

Figure 8 Potentiodynamic polarization curves for S200D Be and (0001), {1*1*00}, and {11*2*0} single crystal Be samples in pH 12.5 sodium hydroxide.